MATLAB Programs for the Analysis of Orographic Precipitation and Isotopes, with Implications for the Study of Paleotopography

Mark T. Brandon
Department of Earth and Planetary Sciences, Yale University, P.O. Box 8109, New Haven CT 06520-8109, United States, email: mark.brandon@yale.edu

Overview

The Orographic Precipitation and Isotopes (OPI) model provides a representation of precipitation and isotope fractionation associated with steady atmospheric flow over an arbitrary three-dimensional topography. The OPI model builds on an earlier precipitation model by Smith and Barstad (2004), which I call LTOP, based on the title of their paper, "A Linear Theory of Orographic Precipitation". The OPI programs are entirely new and have important modifications relative to the LTOP program developed by Smith and Barstad. The most significant modifications are:

1) The LTOP model focuses on the case where loss due to precipitation is small relative to the flux of atmospheric water vapor. The OPI model includes a full mass balance for water vapor, precipitation, and evaporation.
2) The Euler equations for the wind field are defined relative to a uniform moist buoyant stability, where the moist buoyancy frequency, N_m, is constant (Durran and Klemp, 1982). The LTOP model is only approximately tied to a uniform N_m.
3) OPI includes a full calculation of the isotopic evolution of atmospheric water vapor, precipitation, and evaporation.
4) opiFit provides a method to use δ^2H and $\delta^{18}O$ isotopic data from samples of primary meteoric water to estimate, in a least-squares sense, the mean precipitation and isotope fields at a regional scale caused by orographic lifting.

This document is provided as background for the first public release of the OPI programs, using the Zenodo open-access repository. The document has three parts:
1) An outline of the calculations used in the OPI programs.
2) Definition of terms related to the OPI model.
3) Captions to describe the figures produced by the OPI programs.

A separate document in this release provides a synthetic example of an OPI calculation, based on Gaussian-shaped mountain range.

This submission is supplemented by two real applications, involving the study of modern precipitation isotopes in and adjacent to the Patagonian Andes and the Mendoza region in the South-Central Andes (Brandon et al., 2022b, 2022c). Those examples include supporting data, and run files, thus can be used by individuals to see how the programs work. The Patagonia Andes case is used in Chang et al. (2022) to discuss the influence of evaporation on modern precipitation isotopes from that area. The South-Central Andes case is used in Fennell et al. (2022) as a basis for the interpreting of precipitation isotope measurements from Cenozoic samples of hydrated volcanic glass. The research focus there is the interpretation of the Cenozoic topographic evolution of area of Argentina east of the main Andes.

Note that the OPI programs are all written in Matlab, and can be run in those computing environments supported by the Matlab app. This release of OPI includes eleven programs (main functions), and 37 supporting functions. I have tried to write these functions so that there is a minimum dependence on add-on toolboxes. An obvious exception is the Parallel Computing Toolbox, which is required if you want to use opiFit with a cluster of CPUs.

An Outline of Calculations Used by the OPI Model

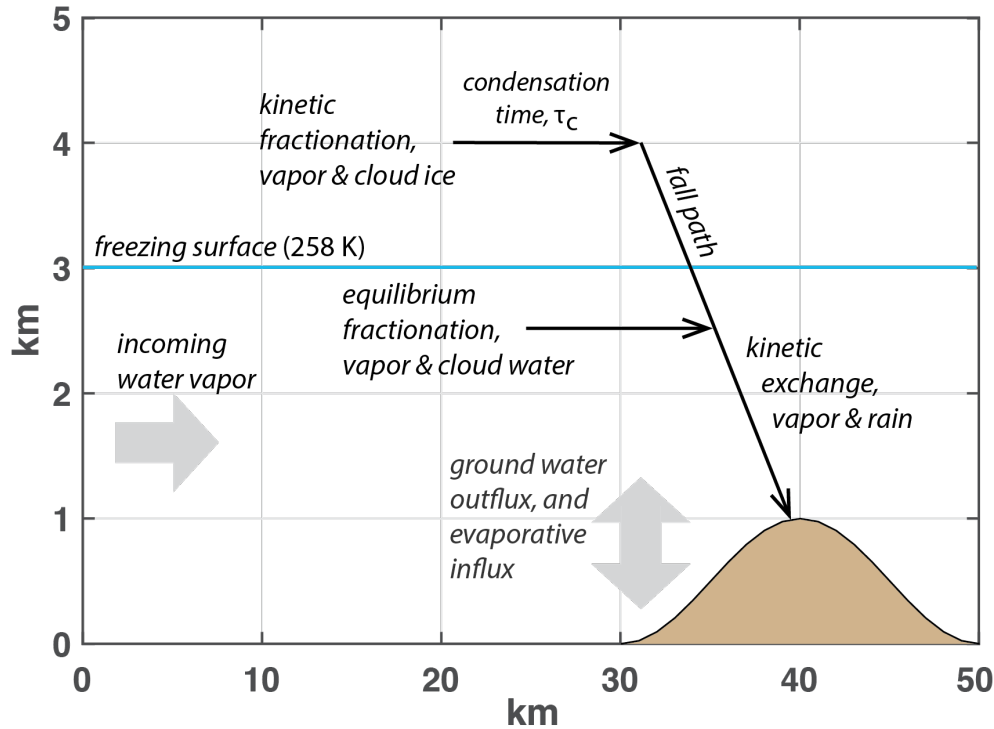Figure 1 shows a schematic of the calculations used in the OPI model. The main features of this model are:

Figure 1. Schematic of the processes represented in the OPI model.

1) The steady wind field in the OPI model is calculated using the moist anelastic formulation for the Euler equations in Durran and Klemp (1982). The base-state for the atmosphere is set to be moist (fully saturated) with a uniform moist buoyancy frequency, N_m, and a sea-level surface-air temperature, T_0. These two parameters are sufficient to define vertical 1D profiles for saturated water vapor density and environmental temperature associated with the base state.

2) The local rates for formation of cloud water and precipitation are based on the orographic precipitation model of Smith and Barstad (2004).

3) The freezing surface is set to 258 K, which marks the center of the Wegener-Bergeron-Findeisen (WBF) zone (268 - 248 K). The interested reader is referred to Storelvmo and Tan (2015) for a current review of the WBF zone. The isotopic fractionation factors for

2

vapor/water and vapor/ice are set to account for a mixture of water and ice (graupel) within the WBF zone. The mixture is scaled so that the fraction of water in this mixture decreases linearly from one at 268 K and to zero at 248 K.

4) Equilibrium fractionation factors are determined using empirical functions. For hydrogen isotopes, Merlivat and Nief (1967) is used for ice/vapor and water/vapor fractionation for 258 to 273 K, and Majoube (1971) is used for water/vapor fractionation for 273 to 373 K. For oxygen isotopes, Majoube (1970) is used for ice/vapor and water/vapor for 240 to 273 K, and Majoube (1971) is used for water/vapor for 273 to 373 K. The isotopic fractionation of ice with respect to vapor includes a kinetic effect. The kinetic model of Cias and Jouzel (1994) is used to calculate the effective fractionation factor for ice/vapor. For this calculation, the diffusivity ratios for the water isotopologues are from Merlivat (1978).

5) OPI accounts for the resetting of the isotopic composition of rain below the freezing level using the method from Friedman et al. (1962). The characteristic time for this process is set to 90 seconds (Lee et al., 2007), which is equivalent to a characteristic fall distance of 540 m, given an average fall velocity for rain of 6 m/s.

6) Return of water vapor back to the atmosphere due to evaporation of precipitation as it falls through the base of the atmosphere is accounted for in OPI. The calculation is based on Criss, (1999, p. 154-159, 175), and uses the diffusivity ratios for water isotopologues from Merlivat (1978).

7) The path integration for the isotopic evolution of the atmosphere along a wind path is accomplished by first calculating an average fractionation factor for the precipitation fall path above each surface point along the wind path. This average uses the water vapor density as a weighting factor, and accounts for temperature along the fall path, isotopic resetting below the WBF zone, and evaporative recycling at the base of the atmosphere. The fall-path averaged fractionation factors are then numerically integrated along the wind path using eq. 3.27 from Criss (1999).

8) Water isotopes can be reported as local values, or catchment-integrated values. Catchment values are calculated as a precipitation-weighted average for water falling in the catchment upslope of the specified location. OPI includes an algorithm that calculates the catchment area using the same topographic grid used for calculating the orographic precipitation.

Definitions
OPI model: Abbreviation for "Orographic Precipitation and Isotopes". OPI refers to the model used to calculate the steady flow of moist air over a specified three-dimensional topography, and the precipitation and isotopic fractionation that is associated with that flow. The OPI model is controlled by 9 parameters: mean wind speed U, mean wind direction *azimuth*, sea-level surface-air temperature T_0, mountain-height number M, horizontal eddy diffusivity κ, mean residence time for cloud water τ_c, the hydrogen isotopic composition of base precipitation at the centroid of the sample data δ^2H_0, the latitudinal gradient of hydrogen isotopic composition of base precipitation $d(\delta^2H) / d(latitude)$, and the fraction of precipitation remaining after evaporation f_p.

The current version of the OPI model can calculate a single one-wind solution in about 2 minutes using a single CPU on the current varieties of personal computers (e.g., 2019 MacBook Pro). I generally use a 1 km grid for the topography, and the gridded results, such as precipitation rate and precipitation isotopes, are returned with the same grid resolution.

opiFit: A program that uses a search model to find the set of OPI parameters that produce the best fit of the OPI model to a set of δ^2H and $\delta^{18}O$ measurements of meteoric water samples collected across a study area. opiFit is controlled by a user-edited run file (see example below). The best-fit solution is appended to the run file when the program finishes. The program also produces a log file describing the run, and solutions file, which includes all candidate solutions generated during the least-squares search.

opiCalc: A program that takes a set of OPI parameters and calculates the predictions, including gridded fields for precipitation rate, and for the δ^2H and $\delta^{18}O$ composition of the precipitation. opiCalc gets the OPI solution from the run file, and produces a mat file (opiCalc_OneWind_Results.mat, opiCalc_TwoWinds_Results.mat) with the extended results for that solution.

opiPlots: A program that produces plots of results from the opiCalc mat file.

opiMaps: A program that produces maps of results from the opiCalc mat file.

opiPredictCalc and opiPredictPlot: Two programs that predict how the solution for modern precipitation isotopes, as defined by a set of OPI parameters, would vary over geologic time. opiPredict accounts for the influence of the local sea-level surface-air temperature on the isotopic composition of the base precipitation and isotopic fractionation during lifting. opiPredictCalc uses an opiCalc mat file representing an OPI solution for modern precipitation, and an Excel file containing information about present and past samples of precipitation isotopes, and produces an Excel file containing predictions for the samples.

One-wind and two-winds versions of the OPI programs: The OPI programs were first developed to estimate the orographic precipitation and isotopes for steady atmospheric flow with a single wind direction. Our work in the South-Central Andes made it clear that we had to expand the capabilities of the programs to allow for a mixture of two steady wind directions. Thus, there are now two sets of programs, distinguished by the terms "One-Wind" and "Two-Winds". opiFit_One-Wind searches for 9 unknown parameters (as described above for the OPI model). opiFit_Two-Winds solves for a mixture of two One-Wind Solutions, each of which has 9 parameters. The total number of parameters for a Two-Winds solution is 19, given that the last parameter, *fraction*, accounts for the relative amount of precipitation provided by these two precipitation sources. opiFit_One-Wind is able to find a best-solution in about 24 hours when using 27 CPUs in a high-performance computer cluster. opiFit_Two-Winds takes about 1 week using the same number of CPUs.

Base-state atmosphere: The state of the atmosphere at a stationary state ($U = 0$). This base state is fully defined by the sea-level surface-air temperature T_0 and moist-buoyancy frequency N_m.

4

Mountain-height number: A dimensionless number that approximates perturbation in wind speed caused by the highest topography in the model domain. This number is defined by $M = N_m H_{max}/U$, where U is mean horizontal wind speed along the mean wind path, H_{max} is the maximum elevation in the model domain, and N_m is the moist buoyancy frequency.

Moist buoyancy frequency: A measure of the vertical density gradient of a moist atmosphere (moist indicates coexisting water vapor, and water or ice). This measure is also commonly called the moist Brunt-Väisälä frequency, and is represented by the variable N_m. The atmosphere tends towards a stable state where the air density decreases with increasing elevation. The state is described as neutrally buoyant when $N_m = 0$ (i.e., the vertical density gradient is zero). As N_m increases, the vertical density gradient becomes increasingly negative, which creates an increasing resistance to flow over topography. OPI uses an atmospheric-flow model where N_m is everywhere constant (Durran and Klemp, 1982). The actual value used for N_m is determined as part of the best-fit solution provided by opiFit.

Primary and altered meteoric water: Meteoric water is formed by condensation and precipitation from atmospheric water vapor. The terms *primary* and *altered* indicate the degree to which the water has been affected by subsequent evaporation. The isotope variable "deuterium excess" is defined by $d = \delta^2 H - 8\,\delta^{18}O$ and is used here to distinguish between primary meteoric water ($d_{excess} > 5$ per mil, little to no evaporation after precipitation), and altered meteoric water ($d_{excess} < 5$ per mil, significant evaporation after precipitation).

Local versus catchment sample: The OPI model accounts for the type of sample, whether it was derived from *local* precipitation, or from an upslope *catchment*. Most samples of modern meteoric water are *catchment sample*. A GNIP station is an ideal example of a *local sample*. Predictions for catchment samples are determined by averaging over the grid nodes that lie upslope of the sample location. The average is weighted by the estimated precipitation rate at each grid node.

Base precipitation: Defined as the precipitation that would fall in the absence of topography. Base precipitation is caused by instabilities within the atmosphere (interaction of weather fronts, convective instabilities, etc.) and by cooling as the atmosphere flows from equator to pole.

Isotopic composition for base precipitation: This composition is represented as a linear function of latitude. The least-squares fit estimates the base-precipitation isotopic composition $\delta^2 H_0$ at the centroid of the sample sites, and an isotopic gradient relative to latitude, $d(\delta^2 H) / d(latitude)$.

Reduced chi-square statistic: χ_r^2 is used in opiFit as a measure of the misfit between the model and data. The estimate for χ_r^2 is given by

$$X_r^2 = \frac{1}{n-m} \sum_{i=1}^{n} \frac{(obs_i - pred_i)^2}{SE(obs_i)^2}$$

where the index *i* enumerates 1 to *n* samples, obs_i and $SE(obs_i)$ are the measured value and standard error for the *i*th sample, $pred_i$ is the value predicted by the model for this sample, and *m* is the number of unknown parameters that were estimated to generate the model prediction. X_r^2

has an expected value of one. In other words, we expect that a good fit will have a X_r^2 value close to one.

Standardized residual: The misfit for a least-squares fit is represented by residuals, which represent the difference between each observed value and the predicted value indicated by the least-squares fit. As used here, the standardized residual for the *i*th sample is $|obs_i - pred_i|/\text{SE}(obs_i)$, where SE indicates standard error.

Controlled random search: opiFit uses a controlled random search (CRS) algorithm (Price, 1977, 1987) to search for a set of OPI parameters that have the smallest χ_r^2 value. The search algorithm is implemented in the function fminCRS3, and can run using one or multiple CPUs. The specific algorithm is CRS3 from Price (1987), with modifications by Brachetti et al. (1997) and Jiao et al. (2006). Brachetti et al. (1997) introduced a weighted scheme for calculating centroid and reflection points, and a quadratic estimate to help accelerate convergence to a final solution. Jiao et al. (2006) introduced a simpler three-point calculation for the quadratic estimate.

Maximum lifting: The maximum elevation of the land surface along the path upwind of a sample location. This path calculation is terminated at the horizontal location where the precipitation first separates from its cloud-water source. This end point is determined by an offset upwind along the wind path equal to $\tau_f U$, where τ_f is the average fall time for the precipitation and U is the average horizontal wind speed along the wind path. The maximum lifting calculation accounts for the sample type, whether local or catchment.

Local elevation: The elevation of the land surface at the horizontal location where the precipitation first separates from its cloud-water source (see "maximum lifting" definition for details). The local-elevation calculation accounts for the sample type, whether local or catchment.

Residual precipitation after evaporation: OPI includes an option to estimate evaporative recycling during precipitation. The OPI least-squares fit is based on modeling samples of primary meteoric water, so the samples themselves are considered to be unaffected by evaporation. Nonetheless, falling precipitation will evaporate as it falls through the atmosphere. This recycling generally decreases the amount of isotopic fractionation that occurs per unit of precipitation produced. In other words, the addition of evaporative recycling will cause atmospheric water vapor to progress more rapidly to a heavier (more positive) isotopic composition. In OPI, evaporative recycling is parameterized by f_p, which represents the fraction of produced precipitation that leaves, as ground water, through the base of the model domain. The complement $1-f_p$ represents the fraction lost to evaporative recycling. The influence of this recycling on the isotopic composition of atmospheric water vapor is determined using the method in Criss, 1999 (p. 154-159, and p. 175, with focus on "Evaporation into an Infinite, Humid Atmosphere"). For this calculation, evaporation is assumed to occur at the base of the model domain. The surface relative humidity is defined by a gridded estimate calculated from the OPI solution. The parameter f_p is set as constant across the model domain and is estimated as part of the least-squares solution. This formulation provides a first-order representation of the influence of evaporative recycling on precipitation isotopes.

Captions for Figures Produced by OPI Programs

opiPairPlots
Figure 1. Minimum value of reduced chi-square, χ_r^2, as a function of the search iteration. The plot shows the evolution and convergence of the search for a best-fit solution.

Figure 2. Termination variable ε as a function of the search iteration. The variable ε is calculated at each step of the search, and is defined by the standard deviation for a set of candidate solutions with the smallest χ_r^2 values. The search is terminated when epsilon is less than a user-specified stopping value, epislon0 (red line). The solution with the smallest χ_r^2 value at termination is defined as the best-fit solution.

Figure 3. Pair plots showing solutions with χ_r^2 values that lie within the bivariate 95-percent confidence region for each pair of parameters. The selected solutions are projected from the full parameter space into the two-parameter view provided by each plot. The solutions are plotted in order of decreasing χ_r^2, so that the smallest χ_r^2 solutions are most apparent in the plot. The confidence regions are estimated using the chi2-contour method of Press et al. (2007, p. 812-816).

Figure 4. Pair plot showing χ_r^2 maps for large regions around the best-fit solution, using the same projection and plotting method as described for Figure 3. These plots are helpful for assessing covariance between the parameter estimates, and for judging the convergence of the search and the uniqueness of the best-fit solution.

opiPlots_OneWind
Figure 1. Comparison of observed and predicted isotope values (circles) for samples of primary meteoric water. The predicted values are determined by a least-squares fit of the observed isotopic data to a one-wind OPI model. The fit is considered good if the data follow the 1:1 reference (gray line). The red square shows the estimated composition of base precipitation.

Figure 2. Craig plot showing δ^2H versus δ^{18}O compositions for primary samples. Gray and blue circles show observed and predicted values, respectively. The gray line is the meteoric water line (MWL) as determined by total least squares fit of the observed data. The red point shows the estimated average for the isotopic composition of base precipitation, and the red ellipse shows the estimated standard-deviation variation of that composition. The ellipse shows the covariance of δ^2H and δ^{18}O, which is mainly due to natural stochastic variation (analytical errors are typically much smaller in comparison). The ratio of the principal standard deviations is set to 28.3, as estimated using observed monthly variation for the GNIP station at Coyhaique, Chile. The magnitude and orientation of the principal standard deviations are determined for each run, using the total least-squares method. The best-fit solution uses this result when calculating reduced chi-square (i.e., the residuals for δ^2H and δ^{18}O for each sample are scaled and combined using the covariance matrix corresponding to the standard-deviation ellipse).

Figure 3. Craig plot showing δ^2H versus δ^{18}O compositions for primary and altered samples. The blue circles are predicted values for primary samples, and the red circles are observed values for altered samples. The offset of the altered samples from the MWL (gray line) is due to

evaporation. The dark green line associated with each altered sample shows the path, as predicted by the OPI solution, from a primary composition on the MWL to the observed altered composition. The average slope of the alteration paths is about five, which is a typical for evaporation of meteoric water (Criss, 1999).

Figure 4. Standardized residuals for best-fit solution. The plots here allow inspection of the standard residuals as a function of horizontal location (easting, northing) in the model domain. A good least-squares fit is characterized by magnitudes that are no greater than about three, and that vary independently across the model domain.

Figure 5. Predicted precipitation isotopes (blue circles) for sample locations as a function of maximum lifting. Maximum lifting is approximated by the maximum elevation of the topography along the path upwind of the sample location. The end point for this path calculation is offset upwind to account for the average horizontal advection of the precipitation as it drops along its fall path. Least-squares is used to estimate the best-fit linear fit to the data, as shown by the gray line, and equation in each plot. Precipitation isotope data typically show a tighter linear relationship with respect to maximum lifting, as opposed to local elevation (see figure 6 for comparison). Note that the calculation of the plotted data accounts for the designation for each sample, whether "local" or "catchment".

Figure 6. Predicted precipitation isotopes (blue circles) for sample locations as a function of local elevation, which is defined as the land surface elevation below the point where precipitation first separates from cloud water. This calculation accounts for downwind offset of precipitation along its fall path. See Figure 5 for details about the calculation and layout of the figure.

Figure 7. One-dimensional temperature field for the base-state atmosphere. The base temperature field is solved by vertical integration of the equation of state for a moist atmosphere, starting with a specified sea-level surface-air temperature T0 and an atmosphere with a uniform moist buoyancy frequency Nm. The left plot shows the actual temperature profile, which is called the environmental temperature. The right plot shows the lapse rate (negative vertical temperature gradient) for the environmental temperature profile, and the moist adiabatic lapse rate, which is a reference gradient observed for local vertical displacement of a moist parcel of air. The lapse rates are small near the surface (usually in the range from 4.5 to 6.5 °C/km), and increase to a limiting value of 10 °C/km in the upper atmosphere. The reason is the exponentially decreasing water vapor with elevation. Note that if the parameter Nm were increased, the difference between the moist and environmental lapse rates would increase and the atmosphere would become more stably stratified and resistant to vertical displacements.

opiPlots_TwoWinds
Figure 1. Comparison of observed versus predicted isotope values (circles) for samples of primary meteoric water. The predicted values are determined by a least-squares fit of the observed isotopic data to a one-wind OPI model. The fit is considered good if the data follow the 1:1 reference (gray line). The blue and red colors indicate the spatial location of a sample relative to the drainage divide (generically assigned here to side1 and side2, respectively). The blue and red squares indicate the isotopic compositions predicted by OPI for base precipitation derived from winds blowing into side1 and side2, respectively.

Figure 2. Craig plot showing δ^2H versus δ^{18}O compositions for primary samples. Gray circles mark sample isotope measurements of meteoric water, and the blue and red circles mark the isotopic compositions predicted by the best-fit two-wind solution. The gray line marks the meteoric water line (MWL), as estimated using a total least-squares fit to the sample data. The blue and red squares mark the predicted isotopic composition for base precipitation derived from winds that blow into side1 and side2 of the topography, relative to the drainage divide. The blue and red ellipses are estimated standard-deviation ellipses of the isotopic composition of the base precipitation. This estimated covariance is used to scale the fit of the paired isotopic measurements (δ^2H and δ^{18}O) for each sample location.

Figure 3. Standardized residuals as function of location (easting, northing). These plots are used to assess if the residuals are spatially uncorrelated, which is a fundamental assumption for a least-squares fit. The standardized residual is defined as the difference between the observed and predicted values, divided by the estimated standard error for the observed value. The expectation is that the standardized residuals should have values close to one if the fit is good. The color of the circles, blue and red, once again indicate the location of each sample relative to the drainage divide (side1 versus side2).

Figure 4. Predicted precipitation isotopes (circles) for sample locations versus maximum lifting along the upwind path to each location. Blue and red indicate the location relative to side1 and side2. The lines show estimated linear trends for the data, as separated into blue and red groups. The summary above reports the intercept and slope for each of these estimated "lifting lines". Precipitation isotope data typically show a tighter linear relationship with respect to maximum lifting, as opposed to local elevation (see figure 4 for comparison).

Figure 5. Predicted precipitation isotopes as a function of local elevation. The layout is the same as for figure 4.

opiMaps_OneWind
Figure 1. Topography and sample locations (black circles). A catchment sample is indicated by a red polygon, which indicates the extent of the upslope catchment. A local sample has no red polygon. The black arrow shows the best-fit wind direction. The black line and square indicate the origin and extent of the cross section (origin defined by the user, orientation is parallel to the best-fit wind direction). The thick gray line marks the drainage divide (if provided by the user).

Figure 2. Observed δ^2H composition (colored circles) for samples of primary meteoric water. The color bar on the right indicates the correspondence between symbol color and composition. Other features are the same as for Figure 1.

Figure 3. Observed deuterium-excess, d, for samples of altered meteoric water.

Figure 4. Predicted orographic precipitation rate (mm/h), as indicated by the specified one-wind OPI solution. White regions indicate no precipitation.

Figure 5. Predicted streamlines (red lines) for atmospheric flow, as indicated by the specified one-wind OPI solution. The streamlines start at an elevation of 2000 m at the upwind limit of the model domain.

Figure 6. Cross section of climate state for the specified one-wind OPI solution. Top panel shows topography (brown), air flow (black streamlines), cloud-water distribution (gray), and precipitation fall lines (dotted black lines). The Wegener-Bergeron-Findeisen zone is delimited by the two blue lines, and marks the upward transition in the atmosphere from rain to ice. The center panel shows the predicted orographic precipitation. The bottom panel shows the predicted distribution of δ^2H in precipitation. The dashed line shows the δ^2H composition of base precipitation, which includes an estimated latitudinal gradient. The section is parallel to the wind direction, and the origin is set at a user-specified location.

Figure 7. Predicted δ^2H for orographic precipitation, as indicated by the specified one-wind OPI solution. White regions indicate no precipitation.

Figure 8. Predicted $\delta^{18}O$ for orographic precipitation, as indicated by the specified one-wind OPI solution. White regions indicate no precipitation.

Figure 9. Surface temperature, as indicated for the specified one-wind OPI solution.

Figure 10. Predicted moisture ratio, as indicated for the specified one-wind OPI solution. The atmosphere starts with a moisture ratio of one at the upwind limit of the model domain.

Figure 11. Location of outlier samples. The blue points show all sample locations. Standardized residuals are reported adjacent to those samples that have large misfits (standardized residuals > 3) relative to the best-fit solution.

Figure 12. Surface velocity ratio, u'/U, for the specified one-wind OPI solution, where U is the the mean wind speed, and u' is the perturbation in wind speed relative to the mean for a location at the topographic surface. This map is useful for assessing if the solution is consistent with the linear approximation used to calculate the wind velocity field, and if there are areas with significant blocking. The linear approximation requires that $|u'/U| < 1$, and blocking is indicated when $u'/U > 1$.

opiMaps_TwoWinds
Figure 1. Topography and sample locations (black circles). Blue and red arrows show wind directions for precipitation states #1 and #2, respectively. Red outlines show upslope catchments for catchment samples. Black square marks the user-defined origin for the cross sections. The red line indicates the drainage divide (if provided by the user).

Figure 2. Predicted mean orographic precipitation rate (mm/h), as indicated by a two-winds OPI solution, with both precipitation states combined. White regions indicate no precipitation.

Figure 3. Predicted streamlines (red lines) for atmospheric flow associated with precipitation state #1. The streamlines start at an elevation of 2000 m at the upwind limit of the model domain.

Figure 4. Predicted streamlines (red lines) for atmospheric flow associated with precipitation state #2. The streamlines start at an elevation of 2000 m at the upwind limit of the model domain.

Figure 5. Cross section of precipitation state #1. Top panel shows topography (brown), air flow (black streamlines), cloud-water distribution (gray), and precipitation fall lines (dotted black lines). The Wegener-Bergeron-Findeisen (WBR) zone is delimited by the two blue lines, and marks the upward transition in the atmosphere from rain to ice. The center panel shows the predicted orographic precipitation. The bottom panel shows the predicted distribution of δ^2H in precipitation. The dashed line shows the δ^2H composition of base precipitation, which includes an estimated latitudinal gradient. The section is oriented in the state #1 wind direction. The section is parallel to the wind direction, and the origin is set at a user-specified location.

Figure 6. Cross section for precipitation state #2. See figure 5 for details.

Figure 7. Predicted δ^2H for orographic precipitation with both states combined. White regions indicate no precipitation.

Figure 8. Predicted $\delta^{18}O$ for orographic precipitation with both states combined. White regions indicate no precipitation.

Figure 9. Mix of orographic precipitation sources, which is shown as the fraction of state #1 precipitation relative to the total predicted orographic precipitation. White regions indicate no precipitation.

Figure 10. Predicted orographic precipitation rate (mm/h) for precipitation state #1. White regions indicate no precipitation.

Figure 11. Predicted orographic precipitation rate (mm/h) for precipitation state #2. White regions indicate no precipitation.

Figure 12. Predicted moisture ratio for precipitation state #1. The atmosphere starts with a moisture ratio of one at the upwind limit of the model domain.

Figure 13. Predicted moisture ratio for precipitation state #2. See figure 12 for details.

Figure 14. Predicted δ^2H for precipitation associated with state #1.

Figure 15. Predicted δ^2H for precipitation associated with state #2.

Figure 16. Surface temperature for precipitation state #1.

Figure 17. Surface temperature for precipitation state #2.

Figure 18. Surface velocity ratio, u'/U, for precipitation state #1, where U is the the mean wind speed, and u' is the perturbation in wind speed relative to the mean for a location at the

topographic surface. This map is useful for assessing if the solution is consistent with the linear approximation used to calculate the wind velocity field, and if there are areas with significant blocking. The linear approximation requires that $|u'/U| < 1$, and blocking is indicated when $u'/U > 1$.

Figure 19. Surface velocity ratio, u'/U, for precipitation state #2. See figure 18 for details.

Figure 20. Location of outlier samples. The blue points show all sample locations. Standardized residuals are reported adjacent to those samples that have large misfits (standardized residuals > 3) relative to the best-fit solution.

opiPredict_Plot
Figure 1. Hydrogen isotopic composition of precipitation as a function of age. Top plot: Measured precipitation $\delta^2 H$ values are shown with red points and error bars (analytical uncertainty, +/- 1 standard error). The associated black line shows the long-term variation of these measurements (smoothed using LOWESS regression with a 5 Ma span). The blue points in the lower part of the plot show predicted $\delta^2 H$ precipitation values for each of the samples after accounting for climate at the sample age but otherwise maintaining the topography the same as modern. The associated blue line shows the long-term variation of this predicted reference case (LOWESS regression, 5 Ma span). The gray line at the top of the plot shows the predicted isotopic composition for base precipitation at the latitude of the samples, and account for the difference in climate relative to modern. The associated blue line shows the long-term variation (LOWESS regression, 5 Ma span). Bottom plot: Predicted sea-surface air temperature at the latitude of the samples and as a function of age.

Figure 2. Predicted evolution of Φ_{lift}, which is the ratio of the observed isotopic fractionation estimated for the sample location and age, relative to predicted isotopic fractionation at same location and age but for a topography that remains the same as modern. These fractionations have been corrected for the change in climate with age. The red points show Φ_{lift} for the samples, and the error bars show ± 1 standard error uncertainties. The uncertainties include analytical errors, and errors associated with estimating the influence of temperature on the isotopic composition of base precipitation, and the isotopic fractionation caused by orographic lifting. The black line shows the long-term variation of Φ_{lift} (LOWESS regression, 5 Ma span), and the black dashed line marks $\Phi_{\text{lift}} = 1$, which is the prediction for a topography that remains the same as modern.

References
Brachetti, P., De Felice Ciccoli, M., Di Pillo, G., and Lucidi, S., 1997, A new version of the Price's algorithm for global optimization, Journal of Global Optimization, v. 10, p. 165–184.

Brandon, M.T., 2022a, MATLAB Programs for the Analysis of Orographic Precipitation and Isotopes, with Implications for the Study of Paleotopography, Zenodo open-access repository.

Brandon, M.T., Chang, Q., and Hren, M.T., 2022b, Analysis of orographic precipitation and isotopes in the vicinity of the Patagonian Andes (latitude 54.8 to 40.1 S), Zenodo open-access repository.

Brandon, M.T., Fennell, L.M., and Hren, M.T., 2022c, Analysis of orographic precipitation and isotopes in the vicinity of the South-Central Andes (latitude 37.6 to 32.4 S), Zenodo open-access repository.

Chang, Q., Brandon, M.T., and Hren, M.T., 2022, Topography, Evaporation and Precipitation Isotopes Across the Patagonian Andes (in review).

Ciais, P., & Jouzel, J., 1994. Deuterium and oxygen 18 in precipitation: Isotopic model, including mixed cloud processes, Journal of Geophysical Research: Atmospheres, *99*(D8), 16793–16803.

Criss, R. E., 1999, Principles of stable isotope distribution, Oxford University Press.

Fennell, L.M., Brandon, M.T., and Hren, M.T., 2022, Cenozoic topographic evolution of the Southern Central Andes foreland region as revealed by hydrogen stable isotopes in hydrated volcanic glass (in review).

Friedman, I., Machta, L., and Soller, R., 1962, Water-vapor exchange between a water droplet and its environment, Journal of Geophysical Research, v. 67, p. 2761-2767.

Durran, D., and Klemp, J., 1982, On the effects of moisture on the Brunt–Vaisala frequency: Journal of the Atmospheric Sciences, v. 39, p. 2152–2158.

Jiao, Y.–C., Dang, C., Leung, Y., Hao, Y., 2006. A modification to the new version of the Price's Algorithm for continuous global optimization problems. J Global Optim, v. 36, p. 609–626.

Lee, J.–E., Fung, I., DePaolo, D. J., and Henning, C. C., 2007, Analysis of the global distribution of water isotopes using the NCAR atmospheric general circulation model: Journal of Geophysical Research, v. 112, p. D16306.

Merlivat, L., and Nief, G., 1967, Fractionnement Isotopique Lors Des Changements Detat Solide–Vapeur Et Liquide–Vapeur De Leau a Des Temperatures Inferieures a 0 Degrees C, Tellus, v. 19, p. 122–127.

Majoube, M. (1970). Fractionation factor of ^{18}O between water vapour and ice, *Nature*, v. 226(5252), p. 1242–1242.

Majoube, M. (1971), Fractionnement en oxygne 18 et en deutrium entre l'eau et sa vapeur, J. Chim. Phys., v. 68, p. 1423–1436.

Merlivat, L., 1978, Molecular diffusivities of H^2, ^{16}O, $HD^{16}O$, and $H_2^{18}O$ in gases, Journal of Chemical Physics, v. 69, p. 2864–2871.

Price, W. L., 1977. A controlled random search procedure for global optimisation. The Computer Journal, 20(4), 367–370.

Price, W.L., 1987. Global optimization algorithms for a CAD workstation. Journal of Optimization Theory and Applications, v. 55(1), p.133–146.

Smith, R. B., and Barstad, I., 2004, A Linear Theory of Orographic Precipitation: Journal of the Atmospheric Sciences, v. 61, p. 1377–1391.

Storelvmo, T., and Tan, I., 2015, The Wegener-Bergeron-Findeisen process – Its discovery and vital importance for weather and climate: Meteorologische Zeitschrift, v. 24, p. 455–461.

Press, W. H., Teukolsky, S. A., Vetterling, W. T., and Flannery, B. P., 2007, Numerical recipes: The art of scientific computing: Cambridge University Press.